One His, Two His…The Emerging Roles of Histidine in Cellular Nickel Trafficking

Peter T. Chivers*,[1] Priyanka Basak,[2] and Michael J. Maroney*[2]

[1] Departments of Biosciences and Chemistry, University of Durham, Durham, DH1 3LE, UK; [2]Department of Chemistry, University of Massachusetts, Amherst MA 01002.

*Corresponding Authors. Address review correspondence to:
Prof. Michael J. Maroney
Department of Chemistry
University of Massachusetts-Amherst
Amherst, MA 01003 USA
413-545-4876
Email: mmaroney@chem.umass.edu

ABSTRACT: Biological environments present a complex array of metal-binding ligands. Metal-binding proteins have been the overwhelming focus of study because of their important and well-defined biological roles. Consequently, the presence of functional low molecular weight (LMW) metal-ligand complexes has been overlooked in terms of their roles in metallobiochemistry, particularly within cells. Recent studies in microbial systems have illuminated the different roles of L-histidine in nickel uptake, gene expression, and metalloenzyme maturation. In this focused critical review, these roles are surveyed in the context of the coordination chemistry of Ni(II) ions and the amino acid histidine, and the physico-chemical properties of nickel complexes of histidine. These complexes are fundamentally important to cellular metal homeostasis and further work is needed to fully define their contributions.

Key Words: histidine, nickel-trafficking, homeostasis, low molecular weight ligands, speciation, maturation

I. Introduction

Histidine was discovered *ca.*1896 by Sven Gustaf Hedin[1]. It is one of the 21 amino acids commonly found in proteins. Its biosynthesis involves a 10-step pathway that is mechanistically conserved from prokaryotes to plants [2,3]. However, it is an essential amino acid in animals and must be obtained from the diet. The imidazole sidechain (**Figure 1)** makes His perhaps the most versatile residue in proteins and enzymes. The side chain pK_a of ~6 facilitates roles in acid-base catalysis, covalent catalysis, and pH sensing. As importantly, the deprotonated sidechain is a prominent ligand in metallobiochemistry. A survey of the MeDBA structure database indicates that 52% (916 of 1738 structurally determined metal sites) involve histidine ligation (https://medba.ddtmlab.org/metalloenzymes/metalsiteclass/; using HIS as Chelate Residue search term)[4]. This prevalence reflects the ability of His to coordinate numerous metals (MeDBA analyses structures independent of physiological importance of metal). In terms of Ni enzymes, the N-terminal His residue found in the nickel-dependent superoxide dismutase, NiSOD, plays an outsized role in both nickel acquisition[5] and in redox catalysis by binding to Ni(III) to stabilize the oxidized complex and releasing Ni(II) while maintaining structurally important protein H-bonding interactions[6]. Free L-His is also an important metal ligand; it is a component of the low molecular weight (LMW) pool of ligands[7] that buffers metal ions inside and outside cells, most notably in plants growing in Ni-rich soils[8]. The ability of L-His and other metabolites to bind Ni(II) and other divalent metals with varying stabilities is predicted from the Irving-Williams trend for first row transition metals (Table I)[9]. These low-molecular complexes are likely abundant in cells but less studied than metalloenzymes, due to their less well-defined biological roles. This review focuses on recent advances in understanding the roles of L-His in Ni biochemistry in bacterial systems, both as a free amino acid and as a protein

residue. Particular consideration is given to the effect of LMW complexes on nickel speciation and the implications for mechanisms of Ni-dependent processes (import, regulation, and enzyme assembly).

II. Histidine coordination and Physico-chemical properties of Nickel-Histidine complexes

A. Speciation

Histidine can form tridentate chelates of metal ions in solution, utilizing the amino and carboxylate terminal groups plus the imidazole side chain (**Figure 1**). Ni(II) ions form two such chelates, the cationic 1:1 $Ni(His)^+$ complex and the neutral 2:1 $Ni(His)_2$ complex. The dissociation constants for $Ni(His)^+$ and $Ni(His)_2$ have been determined by isothermal titration calorimetry (ITC) to be K_{d1} = 15 nM and K_{d2} = 0.214 μM[10], for a common biological buffer system (20 mM HEPES, pH 7.5, I=0.1 M). ITC has an advantage over other (isothermal) methods[11,12] used to determine the stepwise binding constants because it provides thermodynamic data useful for understanding why K_{d1} and K_{d2} differ. In this case, the binding of the second His ligand is enthalpically less favorable than the first. Consequently, the fractional component of $Ni(His)^+$ becomes important to consider when $[His]_{total} \leq 1$ μM (**Figure 2**) at environmental Ni concentrations or at higher nickel concentrations when [Ni] ~ [His]. The ability of Ni(II) to support a 1:1 complex differs from other systems that show strong positive cooperativity in His binding when comparing their stability constants under the same conditions (Table I and reference [11]). For example, for Co(II), K_{d1} and K_{d2} are much less different than for Ni(II); K_{d1} = 0.195 μM; K_{d2} = 4.47 μM.

Histidine is usually present at concentrations well above Ni concentrations (≥ 1000-fold; μM to nM) in most physiological environments. In humans, His concentrations range from 60 to 280 μM in the gastrointestinal tract[13], depending on feeding status and specific location. After absorption from the gastrointestinal (GI) tract, the His concentration range narrows to 75 – 125 μM in plasma, for

example[14]. Determinations of bacterial cytosolic [His] range from 45 – 180 μM[15,16], similar to the human digestive tract and human plasma ranges. This range reflects analysis of different species or growth conditions (*e.g.*, carbon source). A much higher His concentration is found in the xylem of Ni-hyperaccumulator plants, where its levels can rise by 40-fold in response to Ni-exposure, up to ≥ 1 mM[8].

Speciation curves over a range of physiological and lower His concentrations (**Figure 2**), show that virtually all the nickel is present as $Ni(His)_2$ (under limiting [Ni] ~ 10 nM). However, the equilibrium between $Ni(His)^+$ and $Ni(His)_2$ has important implications for [Ni(II)] buffering and ternary complex formation between $Ni(His)^+$ and proteins, as any ligand (protein or another small molecule) with an association constant similar to or tighter than $Ni(His)_2$ will compete with $Ni(His)_2$ formation. Additionally, the presence of other amino acids in physiological environments will increase the abundance of additional stable Ni(His)(X) and $Ni(X)_2$ species[12], shifting the Ni(II) concentration at which $Ni(His)^+$ accumulates to much higher values (Section III.C.1).

$Ni(His)_n$ speciation must be considered in the design and interpretation of biological and biophysical experiments. Dilution of a $Ni(His)_2$ stock solution to decrease $[Ni]_{total}$ into typical physiological ranges (sub micromolar) will shift speciation towards $Ni(His)^+$ when $[His]_{total}$ drops < 10 μM (**Figure 2**). Binding affinities and/or rate constants determined using apparent $[Ni(His)_2]$ under these conditions will be inaccurate unless speciation is calculated for each condition. A more rigorous approach is to titrate Ni(II) solutions against different fixed His concentrations, and *vice versa*, taking into account the K_1 and K_2 values[16]. Binding isotherms and/or observed rates obtained under these conditions will have predictable differences that can differentiate between the contribution of different species, $Ni(His)^+$ or $Ni(His)_2$, to the process under examination.

Ni-speciation in a bacterial cytosol exemplifies the importance of considering LMW complexes in many physiological processes. The availability of free Ni ions,

e.g. $Ni(H_2O)_6^{2+}$, will be << 1/cell (1.6 nM) due to the stability of defined LMW complexes, up to quite high total Ni(II) atoms. The practical absence of the hexaaquo species has two significant implications. First, it becomes important to consider differences in metal affinities between proteins and LMW complexes (and their speciation) rather than absolute affinities. Second, kinetic mechanisms for Ni-transfer cannot reasonably consider the hexaaquo species as part of a mechanism and almost certainly involve ternary complex formation/ligand substitution. Exceptions will occur for nickel import in microbial growth niches with low concentrations of organic molecules and/or reduced pH, that limit complex formation.

B. Structure and stereochemistry of $Ni(His)_2$

Two $Ni(His)_2$ complexes have been crystallographically characterized[17,18]. The structures reveal that the tridentate histidine ligand coordinates only in a *facial* geometry and in two of three possible geometric isomers that are constrained by the stereochemistry of L-His. In the first structure, the imidazole rings are in *trans* positions, while the remaining O- and N- donors are in *cis* orientation (*trans*-imidazole or OC-6-32-*bis*-L-histidinatonickel(II)). In the second case, the amino groups occupy *trans* positions (*trans*-amine, or OC-6-23-*bis*--L-histidinatonickel(II)). The remaining possible geometrical isomer of $Ni(His)_2$ is the *trans*-carboxylate (OC-6-13-) (**Figure 1**). Coordination of the carboxylate O-donor and the amino N-donor forms a 5-membered chelate ring and coordination of the imidazole results in additional 6- and 7-membered chelate rings. The imidazole is sterically constrained by the 6-membered chelate ring to coordinate via the δ-N-donor rather than the ε-N-donor frequently observed in Ni(II) coordination by proteins, where ε-N coordination allows the δ-NH to be available for engaging in H-bond donation within the protein. (Notable examples of δ-N coordination in proteins include the active site of NiSOD, where nickel is also coordinated by the δ-N donor of the N-terminal histidine residue, a feature that is enforced by coordination of the N-terminal amine, thus forming the

same 6-membered chelate ring (*vide infra*) and guanidine hydrolase, where both histidine ligands are δ-N coordinated and unsupported by backbone ligands[19].

Ni(II) ions have a d^8 electronic configuration and all known six-coordinate Ni(II) complexes are high-spin, $S = 1$, with two unpaired electrons in anti-bonding d-orbitals ($d_{x^2-y^2}$ and d_{z^2}). This leads to kinetic lability of the coordination complexes. The ligand exchange rate for the octahedral complexes is relatively fast (*e.g.,* $Ni(II)(H_2O)_6^{2+}$ ion is 3.2×10^4 s^{-1} at 25 C)[20] and proceed by mechanisms that are typically dominated by ligand dissociation. This contrasts with planar four-coordinate Ni(II) complexes, which feature a low-spin, $S = 0$ electronic configuration, resulting in much slower rates of ligand exchange that proceed by mechanisms that are dominated by more associative processes and therefore show a strong dependence on the concentration of the incoming ligand[21]. For $Ni(His)_2$, the lability of six-coordinate complexes would be expected to give rise to a mixture of all three geometric isomers in solution, and the crystal structures likely represent the crystallization of the least soluble components of the mixtures. Similarly, for Co(II), a kinetically labile d^7 system ($Co(II)(H_2O)_6^{2+}$ rate of ligand exchange = 3.2×10^6)[22], the crystallization of $Co(His)_2$ reveals the same *trans*-imidazole structure[23]. However oxidation of a solution of $Co(II)(His)_2$ to Co(III), a low-spin d^6, $S = 0$, system that is kinetically inert (aqua ligand exchange rates in mixed ligand complexes are ~ 10^{-5} s^{-1})[22], allows for the chromatographic separation of all three geometric isomers, which were assigned spectroscopically and demonstrates their presence in the Co(II) solution[24,25].

C. $Ni(His)_n$ complexes and metal-transfer

The presence of abundant LMW Ni(II) complexes in physiological environments means that free nickel ions, *e.g.,* $Ni(H_2O)_6^{2+}$, will be present at insignificant concentrations, *e.g.* << 1/cell. Thus, physiologically relevant observed rates of nickel transfer from (and to) LMW complexes will almost certainly proceed through mechanisms that involve formation of a ternary complex between a partially

coordinated low-molecular weight Ni complex, *e.g.*, $Ni(His)^+$, the most stable 1:1 Ni-amino acid complex[12], and the target protein, rather than a mechanism that involves complete dissociation, *e.g.* $Ni(His)_n$ to $Ni(H_2O)_6^{2+}$, prior to association with the target site. The formation of a ternary complex does not preclude internal, potentially rate-limiting intermediate steps that proceed via a dissociative mechanism, as described earlier (Section II.B)

Human serum albumin (HSA) and $Ni(His)_2$ (and $Ni(Asp)_2^{2-}$) have been identified as Ni-binding components in plasma[26]. $Ni(His)_2$ is thermodynamically more stable than Ni-HSA, so Ni binding to HSA will only occur when the $Ni(His)^+$ pool begins to build (**Figure 3a**)[26]. Experiments with tri-peptides that mimic the HSA ATCUN planar metal-binding motif supported a mechanism of direct nickel transfer between $Ni(His)^+$ and Asp-Ala-His[27], or vice versa from Asp-Ala-His[27] or Gly-Gly-His[28] to L-His. A pH-dependence to the observed rates (10^3 to 10^5 s^{-1}) for both directions is linked to the protonation state of a backbone NH in the HSA peptide. This proton must either dissociate to enable transfer of Ni(II) from Ni-His in the ternary complex or associate to facilitate the transfer of Ni from HSA to His. The observed rates are at non-physiological concentrations for His and Ni, but will equate to reasonable turnovers per second in the context of a cell (for example even a few turnovers per second will saturate a binding site present at 10^{-7} M concentration (~160 sites/cell) within minutes. These studies used high micromolar to millimolar $[His]_{total}$, so that when examining Ni transfer to HSA, $Ni(His)^+$ would have been present at submicromolar concentrations. A modest decrease in starting [His] would have substantially increased $Ni(His)^+$ at t_0 (**Figure 3b**) and lead to much higher observed rates as a function of L-His for a loading mechanism involving a ternary complex.

The HSA 4-coordinate planar site is somewhat comparable in ligand composition to the bacterial 4-coordinate binding sites of regulatory proteins NikR[29,30] and InrS[31], and chaperones (*e.g.*, UreG, *vide infra*) that contain His and Cys residues that may require deprotonation before Ni-loading.

More generally, observed rates of Ni-transfer will depend upon the local protonation state (*e.g.* pH), the intrinsic rate constants of the reaction (E_a), and the concentrations of key species (**Figure 4**). A *higher* concentration of L-His at *low* total Ni will favor the LMW complex, and thus the observed rate of the *reverse* reaction (dissociation) upon ternary complex formation (regardless of relative thermodynamic stabilities). Conversely, increasing total Ni will increase the steady state levels of Ni(L) species (**Figure 4**), and increase the observed rate for the forward reaction, regardless of relative thermodynamic stabilities. The practical example of bacterial transcriptional regulation is relevant here, as increasing Ni-LMW complex levels will facilitate the rate of loading of sensors, leading to changes in gene expression. Because the likely physiological lower molecular weight $Ni(L)_2$ complexes are octahedral, formation of Ni(L) will form via dissociation of the second amino acid ligand. The stability (steady state level) of a ternary complex will depend upon the formation constant of this complex relative to the formation constant of the $Ni(L)_2$ complex (as well as concentrations of the protein and second L). The ternary complex should not be so stable that it creates a high activation energy, but should be sufficiently stable to proceed to transfer, rather than dissociate (**Figure 4**). This is discussed further in Section III.C.1.

III. Biological Roles

A. $Ni(His)_n$ complexes as substrates for bacterial Ni uptake

Bacterial cytosolic nickel levels are balanced in part by transcriptionally-regulated uptake and efflux systems. In *E. coli*, the ABC-type permease, NikABCDE[32], and the exporter RcnAB[33], independently act to balance Ni(II) supply and demand within the cell. Many other bacteria have orthologous systems in addition to less specific mechanisms for metal ion transport at higher concentrations[34]. Typical of bacterial ABC-type importers[35,36], NikA is a periplasmic binding domain protein that binds Ni(II) on the periplasmic side of the

cytoplasmic membrane and associates with protein subunits that form a transport channel across the membrane (NikBC). The energy for transport is supplied by ATP hydrolysis catalyzed by ATPases (NikDE). Histidine plays a critical role in NikABCDE-dependent nickel uptake in *E. coli* and by implication in other bacteria that use Nik orthologs[16].

E. coli is a normal resident of the human digestive tract, and thus Ni availability likely reflects its presence in complex with L-histidine (**Figure 2**). Experiments demonstrated that without L-histidine, Ni(II) could not be imported into the cell by NikABCDE (**Figure 5)**[16]. No other LMW complexes (amino or organic acids) could support Ni(II) uptake. Additionally, D-His prevented Ni-uptake, suggesting specific recognition Ni(L-His)$_n$ complex, rather than a non-specific role in Ni(II) solubilization. Studies of the concentration dependence of L-His on Ni(II) transport and NikA binding revealed that it was Ni(L-His)$_2$ that was recognized by *E coli* NikABCDE[16]. Further, it was demonstrated using ^{3}H-labeled L-His, that L-His was co-transported with Ni(II)[16].

NikA is structurally homologous to di- and oligo-peptide periplasmic proteins[37], consistent with recognition of H-bond donor/acceptor groups rather than exclusively coordination of the metal ion. The subsequent crystal structure of the Ni(L-His)$_2$:NikA complex (PDBID 4I8C)[38] revealed a six-coordinate Ni(II) complex coordinated by three different molecules: two L-histidine ligands provide five donors to the Ni(II) center, one tridentate, as in Ni(His)$_2$ (**Figure 1**), and one bidentate, and one imidazole side chain (His416, Nε) from NikA providing the sixth donor[38]. This residue is essential for Ni(II) transport by NikABCDE[39]. Both L- molecules utilize the 6-membered chelate ring formed between the amino group and the δ-N-donor of the L-His imidazole (**Figure 1**). Interestingly, NikA appears to favor binding to the *trans*-carboxylate geometric Ni(His)$_2$ isomer (**Figure 1**), with His416 displacing one L-His carboxylate ligand from one L-His ligand. Despite the homology to oligo- and di-

peptide importers, OppA and DppA, the interactions between NikA and the L-His ligands are distinct from those observed in OppA and DppA structures. Critically, the displaced L-His carboxylate is stabilized by a salt bridge with Arg137 and has an H-bonding interaction with a water molecule that bridges to Tyr402. Other interactions include a π-stacking interaction between one L-His and Tyr398 and an edge-to-face π-interaction between the fully coordinated L-His and Tyr382, with the carboxylate of this L-His molecule positioned for interactions with Arg97 and Arg386[39].

While the NikA binding site stabilizes a specific geometric isomer of Ni(L-His)$_2$, this does not provide a completely structural basis for specific Ni(L-His)$_2$ binding. Cu(II) and Zn(II) cannot form the stable six-coordinate complex with two His ligands, meaning they are poor competitors for Ni(II) import. However, Co(L-His)$_2$ is isostructural and kinetically labile (*vide supra*) and can inhibit Ni(II) import. However, the weaker stability of the Co(L-His)$_2$ species means that it will be inconsequential at physiological Co(II) and L-His concentrations[11] and is consequently not physiologically relevant (*vide supra*)[16].

The extended recognition mechanism of Ni(L-His)$_2$ by *E. coli* NikA was subsequently shown to be a variation on a theme in bacterial Ni import, suggestive of multiple solutions to the same chemical problem as there are key distinctions (still to be verified with experimental data). At one end of the continuum, the *Staphylococcus aureus* protein recognizes a *trans*-amine Ni(L-His)$_2$ complex but does not displace any of the ligands of the complex to directly bind the Ni atom (PDBID 3RQT). Two Arg residues make contacts to the His carboxylates and thus apparently control isomer specificity. The proteins from *Yersinia* and *Helicobacter pylori* are most similar to *E. coli* NikA, binding a Ni(L-His)$_2$ complex and make direct contact with the Ni atom via a His sidechain and an Arg residue to bind a His carboxylate. Interestingly, however, each His sidechain displaces a different L-His ligand atom (amino group in the Yersinia protein and the imidazole group in the Helicobacter protein) and binds a

different geometric isomer (trans-carboxylate in the Yersinia protein) and an all *cis* isomer in the *Helicobacter* protein. Finally, at the other end of the continuum, the *Campylobacter* NikZ protein (PDBID 4OEU)[40] binds $Ni(His)^+$ and uses three His sidechains to complete the coordination sphere and an Arg residue to stabilize/orient the carboxyl group. Recognition of $Ni(His)^+$ implies a critical difference in species distribution of $Ni(His)_n$ to support transport at decent rates.

Different coordination modes of histidine are also possible, such as utilizing only the 7-membered chelate ring formed between the carboxylate group and the δ-N-donor of the histidine imidazole (*Cj* NikZ), or just the 5-membered chelate formed by coordination of the carboxylate and the amino group without coordination of the imidazole (*Hp* CeuE, PDBID 4LS3)[41]. It appears that while L-His is essential to the recognition that Ni(II) is bound, there are many ways to generate the recognition.

B. Ni-ligand complexes and metal-responsive gene expression

Transcriptional regulation is a primary means of controlling metal ion homeostasis in bacteria. A suite of individually specific metal-sensing, DNA-binding proteins ensures selective responses *in vivo* to individual metals (*e.g.*, Mn to Zn) by sensing changes in metal ion availability. Experimental evidence indicates that these sensors are tuned to specific ranges of buffered metal ion concentrations[42], and do not themselves set the content of the labile cytosolic metal pool. These buffered ranges reflect the position of the metal in the Irving-Williams series, *e.g.,* Zn(II) and Ni(II) are buffered to << 1 $M(H_2O)_6^{2+}$ per cell, while Mn(II) and Fe(II) can be present as the $M(H_2O)_6^{2+}$ species.

Bacterial Ni(II) sensors must therefore be thermodynamically competitive with cytosolic LMW complexes in the cytosol, to bind and allosterically respond to Ni(II), and thus regulate gene expression[7,43]. These sensors use His as a main coordinating ligand in either 4-coordinate planar (*e.g.*, $Ni(Cys)(His)_3$; NikR [29] and $Ni(Cys)_2(His)_2$; InrS [31]) or six-coordinate octahedral (*e.g.*, RcnR [44])) geometries.

The cyanobacterial InrS sensor provides key insight into the link between LMW complexes and Ni-responsive gene regulation. InrS binds to DNA in the apo form, while the Ni-bound protein has weaker DNA-affinity, enabling transcription of transporter genes (*e.g., nrsD*, a Ni(II) exporter) that help to balance cytosolic Ni. Mutations of His residues in InrS that reduce Ni affinity by 20 or 10^5-fold show *at most* a 2.5-fold change in Ni content. This discrepancy highlights the role of sensor proteins in detecting Ni content in the pool and regulating gene expression accordingly, and that they do not themselves determine how much Ni is in the cytosol, otherwise there would have been a much larger change in Ni content.

L-His was shown to be the best amino acid competitor for Ni with purified InrS. Using published InrS Ni and DNA-affinities [43], quantitative models for determining DNA occupancy [45], and cytosolic concentrations of Asp and His in *Synechocystis*[43], the response of InrS to increasing levels of Ni in parallel with LMW Ni complex abundances can be modelled (**Figure 6**). From these models, it appears that InrS is poised to respond to the onset of $Ni(Asp)_2^{2-}$, but this will require experimental tests. Critically, speciation modeling can provide insight into the possible molecular basis for detection of Ni in a bacterial cytosol. Additionally, such modeling could predict a range of metalloregulator Ni-affinities that would be considered physiologically relevant, based on free amino acid levels.

C. Ni Enzyme Maturation and Ni-Incorporation

1. Ternary complex formation during NiSOD maturation

NiSOD is a bacterial superoxide dismutase found predominantly in *Streptomyces* and *Synechococcus* species[46], the latter being perhaps the most abundant cells on the planet[47]. The *sodN* gene is expressed as a catalytically inactive pro-enzyme (SodN) that must be N-terminally processed by a specific peptidase, SodX, to expose the His_1 residue that is critical to the structure and

function of the Ni active site (*vide infra*)[48,49]. (Given the abundance of *Synechococcus* species in the oceans, just one such SodN processing event per cell in 24 h would correspond to ≥10^{25} cleavage reactions). This process differs from the assembly of most other Ni enzymes because it does not require a dedicated chaperone system. Instead, L-Histidine plays a key, direct role in the maturation of NiSOD *in vivo*[5].

The discovery and characterization of NiSOD has outpaced identification and dissection of the biological maturation process. Catalytically active NiSOD for biochemical, biophysical, and structural studies was obtained using engineered constructs of *sodN* in which the endogenous leader sequence was replaced with widely used cleavable tags to effect N-terminal processing, followed by addition of Ni(II) to obtain active enzyme[48,50]. Subsequently, heterologous co-expression in *E. coli* of *sodN* with *sodX* (a gene found adjacent to *sodN* in host species) rescued SOD activity in a nickel-dependent manner that demonstrated the role of SodX as specific peptidase and a central role for Ni in the cleavage process[51]. Recent *in vitro* studies using recombinant, purified SodN and SodX proteins were used to dissect the maturation mechanism of NiSOD and revealed the crucial role of Ni(L-His)$_n$ in the process[5].

SodX, a Ser-Lys dyad protease, cleaves SodN at conserved Ala-His linkage[5] Studies of purified SodN cleavage by SodX that the processed, apo-NiSOD was generated in the absence of Ni(II). The resulting apo-NiSOD could be metalated and activated by the simple addition of unbuffered Ni(II) (**Figure 7**, Pathway A)[5]. In contrast, the addition of unbuffered Ni(II) to the cleavage reaction *inhibited* processing of SodN by SodX (**Figure 7**, Pathway B). These two results apparently contradict the Ni-dependent cleavage observed during heterologous co-expression of *sodN* with *sodX*[51].

The apparent conflict between NiSOD maturation *in vitro* and *in vivo* was resolved by considering the potential role of $Ni(His)_n$ complexes in SodN activation *in vivo*. The stabilities of these complexes excludes consideration of unbuffered $Ni(H_2O)_6^{2+}$ as a component of the maturation process. Indeed, $Ni(L\text{-}His)^+$ is more stable than the inhibitory Ni-pro-SodN complex (K_d = ~15 nM versus 21 μM; SodX does not bind with detectable affinity)[5]. Thus, the inhibition of *in vitro* N-terminal SodN cleavage by Ni(II) might be removed in the presence of L-His, a more physiologically relevant condition (**Figure 7**, Pathway C).

Subsequent experiments studies revealed a direct role for L-His in SodN maturation, rather than an indirect role, *e.g.,* reducing non-specific Ni(II) binding to other site[5]. SodX cleavage in the absence of Ni(II) was inhibited by L-His, and cleavage in the presence of Ni(II) and L-His was observed only within a range of L-His concentrations (0.01 to 1.0 mM), that overlap typical physiological concentrations of L-His (45 - 180 μM)[15]. Higher [L-His] (*e.g.,*10 mM) prevented processing in the presence of Ni(II), supporting a requirement for the 1:1 $Ni(His)^+$ complex in processing, likely in Ni(L-His)SodN ternary complex formation (**Figure 7**, Pathway C). D-His did not support SodX-dependent cleavage of SodN, indicating a stereochemical requirement for $Ni(His)^+$ complex formation with SodX and inconsistent with a non-specific role, such as chelation simple chelation (**Figure 7**, Pathway D)[5]. The presence of L-His also conferred metal-specificity on the cleavage reaction, as other first-row divalent metals did not resulting in SodX-dependent SodN processing[5].

Spectroscopic data also supported a key role for a $Ni(L\text{-}His)^+$ complex in SodN maturation. Ni(II)SodN, without L-His present, lacks the UV-Vis spectroscopic features associated with CysS → Ni(II) LMCT[5,48,52,53], and EXAFS spectra of this complex indicated a six-coordinate site without S-coordination of Ni(II), in contrast the to the 4-5 coordinate S-coordinated site in the mature enzyme (**Table II**)[5] The presence of L-His and Ni(II)SodN (without SodX) revealed several changes in the Ni(II) site. The 6-

coordinate, high-spin site switched to 4-5 coordinate and low-spin, with evidence of S-ligands, as in the mature enzyme (**Table II**)[5].

These observations remove the conflict of previous *in vitro* data co-expression of *sodN* and *sodX* in *E. coli.* The inclusion of L-His leads to the formation of a unique complex formed with SodN that more closely resembles that of the Ni site in mature NiSOD, and leads to specificity of Ni incorporation and avoids mis-metalation in a maturation mechanism that features no metallochaperones.

The mechanism for NiSOD maturation must consider the ability of the NiSodN(His) ternary complex to form under physiological conditions, either as a steady state species or transiently as part of an enzyme reaction pathway (an SodX•SodN-Ni(His) complex). Here, the effect of L-Asp on cytosolic speciation was also considered, as the formation of $Ni(His)(Asp)^-$ and $Ni(Asp)_2^{2-}$ complexes will impact both the stability (steady state level) of a NiSodN(His) ternary complex and the [Ni] at which the monovalent $Ni(His)^+$ and Ni(Asp) complexes, necessary for transient complex formation, are observed (**Figure 8**). The His and Asp concentrations in different bacterial cytosols provide insight into potential physiological constraints on NiSOD maturation and may explain the conditions under which NiSOD maturation was observed in *E. coli*[51]. As cyanobacteria and *Streptomyces* have lower Asp and His concentrations than *E. coli*, the ternary complex becomes detectable at steady state levels at low total Ni atoms/cell (< 100 versus ~450) and the $Ni(L\text{-}His)^+$ species becomes detectable at ~760 Ni/atoms cell compared to ~4800 in *E. coli*. This modeling comparison has not been rigorously tested, but the maturation of heterologously expressed SodN by SodX in *E. coli* required the addition of ≥ 500 μM $NiCl_2$ to the growth medium[51]. This concentration is high enough to result in cytosolic Ni levels sufficient to substantially de-repress Ni efflux by RcnAB [44] and thus correspond to a stress situation in which $Ni(His)^+$ and/or the ternary complex are abundant and able to participate in SodN maturation.

2. Metallochaperones and His-rich proteins

In contrast to NiSOD activation, numerous Ni-enzymes utilize specific chaperones to deliver Ni to the cofactor binding site. Histidine ligands play a critical role in the delivery of Ni(II) to the active sites of nickel-dependent enzymes. This role of protein L-His residues is perhaps best illustrated by the maturation of the enzyme urease, which catalyzes the first step in the hydrolysis of urea[54]. The maturation of urease involves complexes formed between several proteins, UreDFGE (UreD is denoted UreH in *H. pylori*) and apo-urease[55]. A mechanism for Ni(II) incorporation into apo-urease has been rationalized based on the structures of the proteins involved, their protein-protein interactions, and computational modeling[55,56].

$UreE_2$ serves as a Ni metallochaperone in the maturation of urease, delivering Ni(II) to $UreG_2$, which in turn drives delivery to the apo-urease•$Ure(DFG)_2$ complex in a GTP-activated process[55,57,58]. $UreE_2$ binds a single Ni(II) ion with μM affinity at the interface of the homodimeric protein using pairs of His residues provided by the two subunits (**Figure 9**)[59]. One pair is located on the protein surface and the other pair is on flexible C-terminal motifs. At least three of these are bound by the ε-N-imidazole donor. The fourth is disordered in the crystal structure but was detected using XAS, which cannot define the binding mode. Symmetry argues that the two imidazoles in pairs are bound identically, so all four His residues should feature ε-N-imidazole coordination.

UreG is a GTPase and an intrinsically disordered protein that is structurally similar to the hydrogenase accessory protein HypB and binds both Ni(II) and GTP/GDP[55]. Structural studies of $UreG_2$ show that the Ni(II) binding site in $UreG_2$ employs a conserved Cys-Pro-His motif to bind Ni(II) at the dimer interface in a planar four-coordinate *trans*-$(Cys)_2(His)_2$ complex (**Figure 9**) with the His ligands bound by the ε-N imidazole donor[60,61] and with ~70 μM affinity[62]. The presence of both Ni(II) and GTP drives the formation of homodimeric $UreG_2$[56] and the

presence of GTP/GDP also determines the favored protein-binding partner; GTP favors binding to $UreE_2$, while bound GDP favors binding to $Ure(DF)_2$, forming Ure(DFG)[61].. The change in protein binding partner is driven by an allosteric transition that also affects the structure of the Ni(II) binding site; the presence of GTP brings the His ligands into position for formation of the *trans*-$(Cys)_2(His)_2$ complex, while GDP moves them out of position in the Ni(II) binding site[61].

The formation of the $Ure(EG)_2$ creates a novel tight-binding Ni(II) site with nM affinity[63] at the protein interface using the two His residues on the surface of $UreE_2$ and two Cys residues from the conserved Ni binding CPH Ni(II) binding site on $UreG_2$ (**Figure 9**)[64]. Such a tight binding site demands a specific mechanism for release of Ni(II), and it appears likely that the GTPase activity of $UreG_2$ provides this mechanism. It is easy to envision a Ni(II) handoff to $UreG_2$ occurring in the $Ure(EG)_2$ complex in the presence of GTP by substituting the two surface His ligands in $UreE_2$ with the two His ligands in the $UreG_2$ binding site. Hydrolysis of GTP to GDP then drives the formation of $Ure(DFG)_2$ and removes the $UreG_2$ His ligands, setting up a transfer to $UreF_2$ in the $Ure(DFG)_2$ complex. $UreF_2$ is known to bind Ni(II) with μM affinity in a pentacoordinate low-spin site that features exclusively N/O-donor ligands including two His imidazoles[65]. The interface between $UreF_2$ dimer and UreD(H) contains two His residues a Cys residue and three carboxylates that might be involved in binding Ni(II) and ultimately transferring it into trimeric apo-urease active sites bound by UreD(H). It is interesting to note that the urease active site is a dinuclear active site with each Ni(II) ion coordinated by two His ligands[66], and thus Ni(II) can maintain bis-His imidazole coordination throughout the transfer and incorporation process. Such a ligand exchange would be nearly thermodynamically neutral and could be completed without affecting the electronic structure of the Ni(II) center in the partner proteins.

The maturation of urease is more complicated in *H. pylori* than other bacteria because of the use of HypA, another metallochaperone associated with hydrogenase

maturation, in the urease maturation pathway[55]. The tight Ni(II)-binding site found in the $Ure(EG)_2$ complex located at the dimer interface of $UreE_2$ bears some similarity to a complex formed between *H. pylori* $UreE_2$ and HypA[67,68], HypA•$UreE_2$, in that it is a unique Ni site composed of ligands derived from both $UreE_2$ (the two surface His residues) and HypA and has an affinity for Ni(II) (K_d ~ 0.15 nM), (**Figure 9**) [68] far in excess of the μM affinities observed for either $UreE_2$ (*vide supra*) or HypA (K_d ~1 μM)[68]. A combination of spectroscopic, mutagenic data, and computational modelling was used to characterize the Ni(II) binding site of HypA at a conserved N-terminal MHE sequence[69,70]. The data are consistent with coordination of three backbone N-donors, the N-terminal amine and the amidate N-donors from His2 and Glu3, and the imidazole sidechain of His2 (**Figure 9**). The coordination of the backbone N-donors forces coordination of the His2 imidazole by the δ-N-donor, much like coordination of His in the $Ni(His)_2$ complex (*vide supra*). The remaining ligands are provided by the carboxylate of Glu3 and an aquo ligand. Spectroscopic, mutagenic data, and physicochemical characterization provided structural information regarding the high-affinity Ni(II) site in the HypA•$UreE_2$ complex[68]. The data are consistent with the use of three His ligands, with one His derived from HypA (δN-imidazole) along with the two surface His residues of $UreE_2$ (εN-imidazole) that are easily distinguished by hyperfine-shifted ^{1}H-NMR[68], and the bis-amidate and Glu3 carboxylate ligands.

The function of HypA in the hydrogenase maturation pathway is clear: the delivery of Ni(II) to the large subunit of hydrogenase[55]. However, unlike the $Ure(EG)_2$ complex, the physiological role of the HypA•$UreE_2$ complex in urease maturation is not clear. The same pair of His residues on $UreE_2$ is used in forming the high-affinity Ni(II) binding site in both complexes, resulting in a competition between HypA and $UreG_2$ for binding to $UreE_2$[71]. The HypA•$UreE_2$ complex dissociates in favor of the $Ure(EG)_2$ in the presence of GTP and Mg(II), suggesting a

possible mechanism for $UreG_2$ to acquire Ni(II) from HypA via $UreE_2$. This is consistent with the fact that deletion of HypA impairs both hydrogenase and urease maturation, but can be complemented by the addition of Ni(II)[72,73], while deletion of $UreE_2$ prevents urease maturation[73]. Another possibility has to do with the unique role of Ni(II) in the physiology of *H. pylori. H. pylori,* an organism responsible for most gastric ulcers and some cancers[55], is able to survive the acidic environment of the stomach only because it makes urease and uses the ammonia produced by urea hydrolysis to maintain a viable pH[55]. Under neutral conditions, *H. pylori* makes apo-urease and up to 6-15% of the protein content of the cell is urease under all conditions[55]. This apo-urease is rapidly nickelated in response to acid shock[74]. Thus, it is possible that the role of the HypA•$UreE_2$ complex is to prevent incorporation of Ni(II) into urease by blocking transfer of Ni(II) to $UreG_2$ under neutral conditions.

IV Emerging Perspectives

LMW nickel complexes and evolution of Ni-dependent processes.

The abundance and speciation of LMW nickel complexes has implications for the evolution of Ni-enzymes and proteins and their various assembly mechanisms. Some Ni enzymes likely emerged with the earliest cellular life[75,76]. Present day bacteria encode genes for assembly pathways that may not reflect the cellular milieu in which the enzymes first arose, thus the genes may have evolved/been acquired in response to changes in intracellular metal availability. This may give rise to apparent paradoxes in the assembly pathway, for example, if the metal insertion process does not run down a thermodynamic gradient, as seen in vitamin B_{12} biosynthesis[77]. But, extant organisms must contend with LMW Ni-complexes. More recently evolved enzymes[46], such as NiSOD, will have not adapted to changes in LMW buffer species but emerged in their presence. This may account for the direct role of ternary complex formation in SodN maturation (rather than a chaperone assisted deliver

process preceding cleavage, as in NiFe H_2ases). Conversely, the chaperone mediated pathways may have arisen because of the unsuitability of Ni(His)-enzyme ternary complex formation (*e.g.*, cofactor complexity). Similarly, the NikA protein family will have evolved/emerged as the extracellular growth environment became richer in organic ligands, in contrast to free-living bacteria that evolved import systems under less complex speciation conditions.

There are numerous lines of investigation to consider for further study of LMW Ni complexes in bacterial Ni physiology. How do these complexes contribute to mechanisms in the specificity and loading of chaperones in assembly pathways for bi-metallic nickel-enzymes like urease and the more recently identified guanidine hydrolase[19]? (It is worth noting that the published guanidine hydrolase preparation uses 1mM Ni(II) in the assay buffer, suggesting that heterologous expression is a problem for metalation. A similar situation exists for a metformin hydrolase[78].) More broadly, how have LMW complexes affected the successful transfer between bacteria of genes encoding Ni enzymes? NiSOD serves as a general example of how cytosolic metal buffering could limit successful gene transfer, as the levels of Ni ligands in the cytosols of *Synechococcus* and *Streptomyces* make $Ni(His)^+$ and the NiSodN(His) ternary complex more abundant than in *E. coli*. The emergence of a "NiSOD" in a bacterial species with more thermodynamically stable LMW complexes could necessitate a different maturation/assembly process. Critically, the emergence and spread of Ni-enzymes post-GOE, for example, may depend considerably on the speciation of LMW complexes, the absolute abundance of $Ni(His)^+$, and the ability to form stable ternary complexes that lead to subsequent maturation steps under steady state growth conditions that support production of active enzyme under conditions that provide a benefit to the host.

Not all bacteria can synthesize L-His*, e.g.*, some host-associated species like *H. pylori,* which would likely affect the abundance (and regulation) of cytosolic L-His levels. Indeed, cytosolic L-His was not detected in a metabolomics study of bismuth

stress[79]. Interestingly, *H. pylori* express two His-rich proteins, Hpn, that play critical roles in Ni-trafficking[80]. These proteins may complement or substitute for L-His to buffer cytosolic Ni(II). The His-rich sequences of these proteins have weak Ni-dissociation constants (low μM) [81], which will not be competitive with buffered Ni (compare with InrS, K_d, 2.8 x10^{-12} M, **Figure 7**). Nickel affinity measurements have not considered the possibility of ternary complex formation with L-His, for example. As modeled for NiSodN (**Figure 6**), these complexes can accumulate, particularly with increasing total Ni, and would provide a way to substantially expand the buffer capacity by doubling the number of Ni atoms that free L-His could complex - Ni(L-His)$_2$ + Hpn (+ Ni) → 2 Ni(Hpn)(His).

While D-His can be generated biologically in organisms that possess a racemase enzyme[82], it is not expected to be broadly present in physiological environments. Nonetheless, *in vitro* experiments using D-His can help resolve the functional roles of Ni(His)$_n$ complexes beyond a general buffering role. Proteins and enzymes that directly interact with Ni(His)$_n$ complexes should show specificity towards complexes containing L-His but not D-His[5,16].

Experimental data that quantitatively accounts for Ni-speciation in its analysis will improve future understanding of metal homeostasis in cells by enabling the generation of quantitative and mechanistic models for how metal ions are trafficked within cells. The discovery of Asp as a component of the labile LMW pool of nickel ions [7] and the modeling here suggests Asp may need to be considered further as Ni-coordinating residues for proteins with certain functions. The single subunit NixA protein, from *H. pylori* and other bacteria, may provide an example of this. Functional and biophysical studies [83,84] have identified a Ni recognition site that is composed of His and Asp ligands and transmembrane Asp residues that are critical for Ni import, consistent with Asp residues being involved in a relay from the periplasmic to cytoplasmic faces of NixA. Asp is distinct from His in terms of the enthalpy of interaction and net charge of the complex, which may be beneficial in some

environments (*e.g.*, to maintain a neutral, partially hydrated coordination complex ($Ni(Asp)_2(H_2O)_4$ when transiting the helical barrel. Alternatively, or additionally, Asp will remain deprotonated under acidic growth conditions when His ligands may become less useful because of the higher imidazole pK_a.

An experimental focus on the biological contributions of LMW metal-complexes provides an opportunity to generate key insights into inorganic biochemistry in the coming years.

List of abbreviations:

ATCUN - Amino terminal Cu(II)- and Ni(II)

E_a – activation energy

EXAFS – extended x-ray absorption fine structure

ITC – isothermal titration calorimetry

GI - Gastrointestinal

GOE – Great Oxidation Event

HSA – Human serum albumin

K_d – equilibrium dissociation constant

LMCT – ligand-to-metal charge transfer

LMW – low molecular weight

NiSOD – nickel superoxide dismutase

UV-vis – ultraviolet-visible

IV. References

[1] H.B. Vickery, C.S. Leavenworth, ON THE SEPARATION OF HISTIDINE AND ARGININE, J. Biol. Chem. 78 (1928) 627–635. https://doi.org/10.1016/S0021-9258(18)83967-9.

[2] R.A. Ingle, Histidine Biosynthesis, Arab. Book 9 (2011) e0141. https://doi.org/10.1199/tab.0141.

[3] M.E. Winkler, S. Ramos-Montañez, Biosynthesis of Histidine, EcoSal Plus 3 (2009) 10.1128/ecosalplus.3.6.1.9. https://doi.org/10.1128/ecosalplus.3.6.1.9.

[4] J.-L. Yu, S. Wu, C. Zhou, Q.-Q. Dai, C.J. Schofield, G.-B. Li, MeDBA: the Metalloenzyme Data Bank and Analysis platform, Nucleic Acids Res. 51 (2023) D593–D602. https://doi.org/10.1093/nar/gkac860.

[5] P. Basak, D.E. Cabelli, P.T. Chivers, E.R. Farquhar, M.J. Maroney, *In vitro* maturation of NiSOD reveals a role for cytoplasmic histidine in processing and metalation, Metallomics 15 (2023) mfad054. https://doi.org/10.1093/mtomcs/mfad054.

[6] Y. Sheng, I.A. Abreu, D.E. Cabelli, M.J. Maroney, A.-F. Miller, M. Teixeira, J.S. Valentine, Superoxide Dismutases and Superoxide Reductases, Chem. Rev. 114 (2014) 3854–3918. https://doi.org/10.1021/cr4005296.

[7] H.N. Brawley, P.A. Lindahl, Direct Detection of the Labile Nickel Pool in *Escherichia coli* : New Perspectives on Labile Metal Pools, J. Am. Chem. Soc. 143 (2021) 18571–18580. https://doi.org/10.1021/jacs.1c08213.

[8] U. Kramer, J.D. CotterHowells, J.M. Charnock, A.J.M. Baker, J.A.C. Smith, Free histidine as a metal chelator in plants that accumulate nickel, Nature 379 (1996) 635–638. https://doi.org/10.1038/379635a0.

[9] H. Irving, R.J.P. Williams, Order of stability of metal complexes, Nature 162 (1948) 746–747.

[10] Y. Zhang, D.E. Wilcox, Thermodynamic and spectroscopic study of Cu(II) and Ni(II) binding to bovine serum albumin, J Biol Inorg Chem 7 (2002) 327–37.

[11] D.D. Perrin, V.S. Sharma, Histidine complexes with some bivalent cations, J. Chem. Soc. Inorg. Phys. Theor. (1967) 724. https://doi.org/10.1039/j19670000724.

[12] J.R. Blackburn, M.M. Jones, Stereoselectivity in the metal complex catalyzed hydrolysis of amino acid esters — III Distribution equilibria, J. Inorg. Nucl. Chem. 35 (1973) 1605–1620. https://doi.org/10.1016/0022-1902(73)80252-0.

[13] S.A. Adibi, D.W. Mercer, Protein digestion in human intestine as reflected in luminal, mucosal, and plasma amino acid concentrations after meals, J Clin Invest 52 (1973) 1586–94.

[14] J.K. Teloh, D.-S. Dohle, M. Petersen, R. Verhaegh, I.N. Waack, F. Roehrborn, H. Jakob, H. De Groot, Histidine and other amino acids in blood and urine after administration of Bretschneider solution (HTK) for cardioplegic arrest in patients: effects on N-metabolism, Amino Acids 48 (2016) 1423–1432. https://doi.org/10.1007/s00726-016-2195-2.

[15] B.D. Bennett, E.H. Kimball, M. Gao, R. Osterhout, S.J. Van Dien, J.D. Rabinowitz, Absolute metabolite concentrations and implied enzyme active site occupancy in Escherichia coli, Nat Chem Biol 5 (2009) 593–9. https://doi.org/10.1038/nchembio.186.

[16] P.T. Chivers, E.L. Benanti, V. Heil-Chapdelaine, J.S. Iwig, J.L. Rowe, Identification of Ni-(L-His)(2) as a substrate for NikABCDE-dependent nickel uptake in Escherichia coli, Metallomics 4 (2012) 1043–50. https://doi.org/10.1039/c2mt20139a.

[17] K.A. Fraser, M.M. Harding, The Crystal and Molecular Structure of Bis(histidino)nickel(II) Monohydrate, J Chem Soc (1967) 415–420.

[18]A. Abbasi, B. Safarkoopayeh, N. Khosravi, A. Shayesteh, CCDC 979056: Experimental Crystal Structure Determination, (2017). https://doi.org/10.5517/CCDC.CSD.CC11VSG4.
[19]D. Funck, M. Sinn, J.R. Fleming, M. Stanoppi, J. Dietrich, R. López-Igual, O. Mayans, J.S. Hartig, Discovery of a Ni2+-dependent guanidine hydrolase in bacteria | Nature, Nature 603 (2022) 515–521. https://doi.org/10.1038/s41586-022-04490-x.
[20]H. Diebler, M. Eigen, G. Ilgenfritz, G. Maass, R. Winkler, Kinetics and mechanism of reactions of main group metal ions with biological carriers, Pure Appl. Chem. 20 (1969) 93–116. https://doi.org/10.1351/pac196920010093.
[21]J.A. Casares, P. Espinet, J.M. Martínez-Ilarduya, J.J. Mucientes, G. Salas, Study of the Replacement of Weak Ligands on Square-Planar Organometallic Nickel(II) Complexes. Organo-Nickel Aquacomplexes, Inorg. Chem. 46 (2007) 1027–1032. https://doi.org/10.1021/ic061933k.
[22]L. Helm, A.E. Merbach, Inorganic and bioinorganic solvent exchange mechanisms, Chem Rev 105 (2005) 1923–59.
[23]M.M. Harding, H.A. Long, Crystal and Molecular Structure of Bis-(L-hitidino)cobalt(II) Monohydrate, J Chem Soc (1968) 2554–2559.
[24]L.J. Zompa, Preparation and Tentative Structural Assignment of Geometrical Isomers of Bis-(L-Histidinato)Cobalt(3) Ion, J. Chem. Soc. -Chem. Commun. (1969) 783-. https://doi.org/10.1039/C29690000783.
[25]S. Bagger, K. Gibson, C.S. Sørensen, The Isomerism of Cobalt(III) Histindinato Chelates, Acta Chem Scand 26 (1972) 2503–2510.
[26]M. Lucassen, B. Sarkar, Nickel(II)-binding constituents of human blood serum, J Toxicol Env. Health 5 (1979) 897-905.
[27]M. Tabata, B. Sarkar, Specific nickel(II)-transfer process between the native sequence peptide representing the nickel(II)-transport site of human serum albumin and L-histidine, J Inorg Biochem 45 (1992) 93-104.
[28]R.W. Hay, M.M. Hassan, C. You-Quan, Kinetic and thermodynamic studies of the copper(II) and nickel(II) complexes of glycylglycyl-L-histidine, J. Inorg. Biochem. 52 (1993) 17–25. https://doi.org/10.1016/0162-0134(93)85619-J.
[29]E.R. Schreiter, M.D. Sintchak, Y. Guo, P.T. Chivers, R.T. Sauer, C.L. Drennan, Crystal structure of the nickel-responsive transcription factor NikR, Nat Struct Biol 10 (2003) 794–9.
[30]E.R. Schreiter, S.C. Wang, D.B. Zamble, C.L. Drennan, NikR-operator complex structure and the mechanism of repressor activation by metal ions, Proc. Natl. Acad. Sci. U. S. A. 103 (2006) 13676–81. https://doi.org/0606247103 [pii] 10.1073/pnas.0606247103.
[31]C.E. Carr, A.W. Foster, M.J. Maroney, An XAS investigation of the nickel site structure in the transcriptional regulator InrS, J. Inorg. Biochem. 177 (2017) 352–358. https://doi.org/10.1016/j.jinorgbio.2017.08.003.
[32]F. Kirsch, T. Eitinger, Transport of nickel and cobalt ions into bacterial cells by S components of ECF transporters, Biometals 27 (2014) 653–60. https://doi.org/10.1007/s10534-014-9738-3.
[33]J.S. Iwig, J.L. Rowe, P.T. Chivers, Nickel homeostasis in Escherichia coli - the rcnR-rcnA efflux pathway and its linkage to NikR function, Mol Microbiol 62 (2006) 252–62. https://doi.org/10.1111/j.1365-2958.2006.05369.x.
[34]T. Eitinger, Nickel Transporters, in: R.H. Kretsinger, V.N. Uversky, E.A. Permyakov (Eds.), Encycl. Met., Springer New York, New York, NY, 2013: pp. 1515–1519. https://doi.org/10.1007/978-1-4614-1533-6_85.
[35]D.C. Rees, E. Johnson, O. Lewinson, ABC transporters: the power to change, Nat Rev Mol Cell Biol 10 (2009) 218–27.
[36]P. Zhang, Structure and mechanism of energy-coupling factor transporters, Trends Microbiol 21 (2013) 652–9. https://doi.org/10.1016/j.tim.2013.09.009.

[37]R.P.-A. Berntsson, S.H.J. Smits, L. Schmitt, D.-J. Slotboom, B. Poolman, A structural classification of substrate-binding proteins, FEBS Lett. 584 (2010) 2606–2617. https://doi.org/10.1016/j.febslet.2010.04.043.
[38]H. Lebrette, M. Iannello, J.C. Fontecilla-Camps, C. Cavazza, The binding mode of Ni-((L)-His)(2) in NikA revealed by X-ray crystallography, J Inorg Biochem 121C (2012) 16–18. https://doi.org/10.1016/j.jinorgbio.2012.12.010.
[39]C. Cavazza, L. Martin, E. Laffly, H. Lebrette, M.V. Cherrier, L. Zeppieri, P. Richaud, M. Carriere, J.C. Fontecilla-Camps, Histidine 416 of the periplasmic binding protein NikA is essential for nickel uptake in *Escherichia coli*, FEBS Lett. 585 (2011) 711–5. https://doi.org/S0014-5793(11)00070-6 [pii] 10.1016/j.febslet.2011.01.038.
[40]H. Lebrette, C. Brochier-Armanet, B. Zambelli, H. de Reuse, E. Borezee-Durant, S. Ciurli, C. Cavazza, Promiscuous nickel import in human pathogens: structure, thermodynamics, and evolution of extracytoplasmic nickel-binding proteins, Structure 22 (2014) 1421–32. https://doi.org/10.1016/j.str.2014.07.012.
[41]M.M. Shaik, L. Cendron, M. Salamina, M. Ruzzene, G. Zanotti, Helicobacter pylori periplasmic receptor CeuE (HP1561) modulates its nickel affinity via organic metallophores, Mol Microbiol 91 (2014) 724–35. https://doi.org/10.1111/mmi.12487.
[42]D. Osman, M.A. Martini, A.W. Foster, J. Chen, A.J.P. Scott, R.J. Morton, J.W. Steed, E. Lurie-Luke, T.G. Huggins, A.D. Lawrence, E. Deery, M.J. Warren, P.T. Chivers, N.J. Robinson, Bacterial sensors define intracellular free energies for correct enzyme metalation, Nat Chem Biol (2019) in press.
[43]A.W. Foster, R. Pernil, C.J. Patterson, A.J.P. Scott, L.O. Palsson, R. Pal, I. Cummins, P.T. Chivers, E. Pohl, N.J. Robinson, A tight tunable range for Ni(II) sensing and buffering in cells, Nat Chem Biol 13 (2017) 409–414. https://doi.org/10.1038/nchembio.2310.
[44]J.S. Iwig, S. Leitch, R.W. Herbst, M.J. Maroney, P.T. Chivers, Ni(II) and Co(II) sensing by Escherichia coli RcnR, J Am Chem Soc 130 (2008) 7592–606. https://doi.org/10.1021/ja710067d.
[45]D. Osman, C. Piergentili, J. Chen, B. Chakrabarti, A.W. Foster, E. Lurie-Luke, T.G. Huggins, N.J. Robinson, Generating a Metal-responsive Transcriptional Regulator to Test What Confers Metal Sensing in Cells, J Biol Chem 290 (2015) 19806–22. https://doi.org/10.1074/jbc.M115.663427.
[46]C.L. Dupont, K. Neupane, J. Shearer, B. Palenik, Diversity, function and evolution of genes coding for putative Ni-containing superoxide dismutases, Env. Microbiol 10 (2008) 1831–43.
[47]P. Flombaum, J.L. Gallegos, R.A. Gordillo, J. Rincón, L.L. Zabala, N. Jiao, D.M. Karl, W.K.W. Li, M.W. Lomas, D. Veneziano, C.S. Vera, J.A. Vrugt, A.C. Martiny, Present and future global distributions of the marine Cyanobacteria *Prochlorococcus* and *Synechococcus*, Proc. Natl. Acad. Sci. 110 (2013) 9824–9829. https://doi.org/10.1073/pnas.1307701110.
[48]P.A. Bryngelson, S.E. Arobo, J.L. Pinkham, D.E. Cabelli, M.J. Maroney, Expression, Reconstitution and Mutation of Recombinant Streptomyces coelicolor NiSOD, J Am Chem Soc 126 (2004) 460–461.
[49]E.-J. Kim, H.-J. Chung, B. Suh, Y.C. Hah, J.-H. Roe, Transcriptional and post-transcriptional regulation by nickel of sodN gene encoding nickel -containing superoxide dismutase from Streptomyces coelicolor Muller, Mol. Microbiol. 27 (1998) 187–195.
[50]D.P. Barondeau, C.J. Kassmann, C.K. Bruns, J.A. Tainer, E.D. Getzoff, Nickel Superoxide Dismutase Structure and Mechanism, Biochemistry 43 (2004) 8038–8047.
[51]T. Eitinger, In vivo production of active nickel superoxide dismutase from Prochlorococcus marinus MIT9313 is dependent on its cognate peptidase, J Bacteriol 186 (2004) 7821–7825.

[52]A.T. Fiedler, P.A. Bryngelson, M.J. Maroney, T.C. Brunold, Spectroscopic and Computational Studies of Ni Superoxide Dismutase: Electronic Structure Contributions to Enzymatic Function, J Am Chem Soc 127 (2005) 5449–5462.
[53]S.B. Choudhury, J.-W. Lee, G. Davidson, Y.-I. Yim, K. Bose, M.L. Sharma, S.-O. Kang, D.E. Cabelli, M.J. Maroney, Examination of the Nickel Site Structure and Reaction Mechanism in Streptomyces seoulensis Superoxide Dismutase, Biochemistry 38 (1999) 3744–3752.
[54]M.J. Maroney, S. Ciurli, Nonredox Nickel Enzymes, Chem. Rev. 114 (2014) 4206–4228. https://doi.org/Doi 10.1021/Cr4004488.
[55]M.J. Maroney, S. Ciurli, Nickel as a virulence factor in the Class I bacterial carcinogen, Helicobacter pylori, Semin. Cancer Biol. 76 (2021) 143–155. https://doi.org/10.1016/j.semcancer.2021.04.009.
[56]Y.H. Fong, H.C. Wong, M.H. Yuen, P.H. Lau, Y.W. Chen, K.B. Wong, Structure of UreG/UreF/UreH complex reveals how urease accessory proteins facilitate maturation of Helicobacter pylori urease, PLoS Biol 11 (2013) e1001678. https://doi.org/10.1371/journal.pbio.1001678.
[57]A. Soriano, R.P. Hausinger, GTP-dependent activation of urease apoprotein in complex with the UreD, UreF, and UreG accessory proteins, Proc. Natl. Acad. Sci. U. S. A. 96 (1999) 11140–11144.
[58]X.M. Yang, H.Y. Li, T.P. Lai, H.Z. Sun, UreE-UreG Complex Facilitates Nickel Transfer and Preactivates GTPase of UreG in Helicobacter pylori, J. Biol. Chem. 290 (2015) 12474–12485. https://doi.org/10.1074/jbc.M114.632364.
[59]K. Banaszak, V. Martin-Diaconescu, M. Bellucci, B. Zambelli, W. Rypniewski, M.J. Maroney, S. Ciurli, Crystallographic and X-ray absorption spectroscopic characterization of *Helicobacter pylori* UreE bound to Ni^{2+} and Zn^{2+} reveals a role for the disordered C-terminal arm in metal trafficking, Biochem J 441 (2012) 1017–26. https://doi.org/BJ20111659 [pii] 10.1042/BJ20111659.
[60]V. Martin-Diaconescu, M. Bellucci, F. Musiani, S. Ciurli, M.J. Maroney, Unraveling the Helicobacter pylori UreG zinc binding site using X-ray absorption spectroscopy (XAS) and structural modeling, J. Biol. Inorg. Chem. 17 (2012) 353–361. https://doi.org/10.1007/s00775-011-0857-9.
[61]M.H. Yuen, Y.H. Fong, Y.S. Nim, P.H. Lau, K.-B. Wong, Structural insights into how GTP-dependent conformational changes in a metallochaperone UreG facilitate urease maturation, Proc. Natl. Acad. Sci. 114 (2017). https://doi.org/10.1073/pnas.1712658114.
[62]A. Pierro, E. Etienne, G. Gerbaud, B. Guigliarelli, S. Ciurli, V. Belle, B. Zambelli, E. Mileo, Nickel and GTP Modulate Helicobacter pylori UreG Structural Flexibility, Biomolecules 10 (2020) 1062. https://doi.org/10.3390/biom10071062.
[63]M. Bellucci, B. Zambelli, F. Musiani, P. Turano, S. Ciurli, Helicobacter pylori UreE, a urease accessory protein: specific Ni^{2+}- and Zn^{2+}-binding properties and interaction with its cognate UreG, Biochem. J. 422 (2009) 91–100. https://doi.org/BJ20090434 [pii] 10.1042/BJ20090434.
[64]A. Merloni, O. Dobrovolska, B. Zambelli, F. Agostini, M. Bazzani, F. Musiani, S. Ciurli, Molecular landscape of the interaction between the urease accessory proteins UreE and UreG, Biochim. Biophys. Acta-Proteins Proteomics 1844 (2014) 1662–1674. https://doi.org/10.1016/j.bbapap.2014.06.016.
[65]B. Zambelli, A. Berardi, V. Martin-Diaconescu, L. Mazzei, F. Musiani, M.J. Maroney, S. Ciurli, Nickel binding properties of Helicobacter pylori UreF, an accessory protein in the nickel-based activation of urease, JBIC J. Biol. Inorg. Chem. 19 (2014) 319–334. https://doi.org/10.1007/s00775-013-1068-3.
[66]L. Mazzei, F. Musiani, S. Ciurli, The structure-based reaction mechanism of urease, a nickel dependent enzyme: tale of a long debate, JBIC J. Biol. Inorg. Chem. 25 (2020) 829–845. https://doi.org/10.1007/s00775-020-01808-w.

[67] H.Q. Hu, H.T. Huang, M.J. Maroney, The Helicobacter pylori HypA.UreE2 Complex Contains a Novel High-Affinity Ni(II)-Binding Site, Biochemistry (2018). https://doi.org/10.1021/acs.biochem.8b00127.
[68] B. Zambelli, P. Basak, H. Hu, M. Piccioli, F. Musiani, V. Broll, L. Imbert, J. Boisbouvier, M.J. Maroney, S. Ciurli, The structure of the high-affinity nickel-binding site in the Ni,Zn-HypA•UreE2 complex, Metallomics 15 (2023) mfad003. https://doi.org/10.1093/mtomcs/mfad003.
[69] H.D.Q. Hu, R.C. Johnson, D.S. Merrell, M.J. Maroney, Nickel Ligation of the N-Terminal Amine of HypA Is Required for Urease Maturation in Helicobacter pylori, Biochemistry 56 (2017) 1105–1116. https://doi.org/10.1021/acs.biochem.6b00912.
[70] C.A.E.M. Spronk, S. Żerko, M. Górka, W. Koźmiński, B. Bardiaux, B. Zambelli, F. Musiani, M. Piccioli, P. Basak, F.C. Blum, R.C. Johnson, H. Hu, D.S. Merrell, M. Maroney, S. Ciurli, Structure and dynamics of Helicobacter pylori nickel-chaperone HypA: an integrated approach using NMR spectroscopy, functional assays and computational tools, JBIC J. Biol. Inorg. Chem. 23 (2018) 1309–1330. https://doi.org/10.1007/s00775-018-1616-y.
[71] S.L. Benoit, J.L. McMurry, S.A. Hill, R.J. Maier, Helicobacter pylori hydrogenase accessory protein HypA and urease accessory protein UreG compete with each other for UreE recognition, Biochim. Biophys. Acta 1820 (2012) 1519–25. https://doi.org/S0304-4165(12)00169-9 [pii] 10.1016/j.bbagen.2012.06.002.
[72] J.W. Olson, N.S. Mehta, R.J. Maier, Requirement of nickel metabolism proteins HypA and HypB for full activity of both hydrogenase and urease in Helicobacter pylori (vol 39, pg 176, 2001), Mol. Microbiol. 40 (2001) 270–270. https://doi.org/DOI 10.1046/j.1365-2958.2001.02397.x.
[73] S.L. Benoit, A.L. Zbell, R.J. Maier, Nickel enzyme maturation in Helicobacter hepaticus: roles of accessory proteins in hydrogenase and urease activities, Microbiology 153 (2007) 3748–3756. https://doi.org/10.1099/mic.0.2007/010520-0.
[74] K. Stingl, H. De Reuse, Staying alive overdosed: how does Helicobacter pylori control urease activity?, Int J Med Microbiol 295 (2005) 307–15.
[75] E.K. Moore, B.I. Jelen, D. Giovannelli, H. Raanan, P.G. Falkowski, Metal availability and the expanding network of microbial metabolisms in the Archaean eon, Nat. Geosci. 10 (2017) 629–636. https://doi.org/10.1038/ngeo3006.
[76] F.U. Battistuzzi, A. Feijao, S.B. Hedges, A genomic timescale of prokaryote evolution: insights into the origin of methanogenesis, phototrophy, and the colonization of land, BMC Evol. Biol. 4 (2004) 44. https://doi.org/10.1186/1471-2148-4-44.
[77] T.R. Young, E. Deery, A.W. Foster, M.A. Martini, D. Osman, M.J. Warren, N.J. Robinson, Two Distinct Thermodynamic Gradients for Cellular Metalation of Vitamin B_{12}, JACS Au 3 (2023) 1472–1483. https://doi.org/10.1021/jacsau.3c00119.
[78] L.J. Tassoulas, J.A. Rankin, M.H. Elias, L.P. Wackett, Dinickel enzyme evolved to metabolize the pharmaceutical metformin and its implications for wastewater and human microbiomes, Proc. Natl. Acad. Sci. 121 (2024) e2312652121. https://doi.org/10.1073/pnas.2312652121.
[79] B. Han, Z. Zhang, Y. Xie, X. Hu, H. Wang, W. Xia, Y. Wang, H. Li, Y. Wang, H. Sun, Multi-omics and temporal dynamics profiling reveal disruption of central metabolism in *Helicobacter pylori* on bismuth treatment, Chem. Sci. 9 (2018) 7488–7497. https://doi.org/10.1039/C8SC01668B.
[80] H. De Reuse, D. Vinella, C. Cavazza, Common themes and unique proteins for the uptake and trafficking of nickel, a metal essential for the virulence of Helicobacter pylori, Front. Cell. Infect. Microbiol. 3 (2013). https://doi.org/10.3389/fcimb.2013.00094.

[81]D. Witkowska, A. Szebesczyk, J. Wątły, M. Braczkowski, M. Rowińska-Żyrek, A Comparative Study on Nickel Binding to Hpn-like Polypeptides from Two Helicobacter pylori Strains, Int. J. Mol. Sci. 22 (2021) 13210. https://doi.org/10.3390/ijms222413210.
[82]M. Adachi, R. Shimizu, S. Kato, T. Oikawa, The first identification and characterization of a histidine-specific amino acid racemase, histidine racemase from a lactic acid bacterium, Leuconostoc mesenteroides subsp. sake NBRC 102480, Amino Acids 51 (2019) 331–343. https://doi.org/10.1007/s00726-018-2671-y.
[83]J.F. Fulkerson, R.M. Garner, H.L. Mobley, Conserved residues and motifs in the NixA protein of *Helicobacter pylori* are critical for the high affinity transport of nickel ions, J Biol Chem 273 (1998) 235–41.
[84]J.A. Hernandez, P.S. Micus, S.A.L. Sunga, L. Mazzei, S. Ciurli, G. Meloni, Metal selectivity and translocation mechanism characterization in proteoliposomes of the transmembrane NiCoT transporter NixA from *Helicobacter pylori*, Chem. Sci. 15 (2024) 651–665. https://doi.org/10.1039/D3SC05135H.
[85]P. Deschamps, P.P. Kulkarni, B. Sarkar, X-ray structure of physiological copper(II)-bis(L-histidinato) complex, Inorg Chem 43 (2004) 3338–40. https://doi.org/10.1021/ic035413q.
[86]R.H. Kretsinger, F.A. Cotton, R.F. Bryan, The crystal and molecular structure of di-(L-histidino)-zinc (II) dihydrate, Acta Cryst 16 (1963) 651–657.
[87]P. Kuzmic, Program DYNAFIT for the analysis of enzyme kinetic data: application to HIV proteinase, Anal Biochem 237 (1996) 260–73. https://doi.org/10.1006/abio.1996.0238.
[88]K. Momma, F. Izumi, *VESTA 3* for three-dimensional visualization of crystal, volumetric and morphology data, J. Appl. Crystallogr. 44 (2011) 1272–1276. https://doi.org/10.1107/S0021889811038970.

ACKNOWLEDGMENTS
PTC is currently funded by BBSRC grants BB/V006002/1, BB/Y008448/1, and BB/Y008456/1. MJM gratefully acknowledges partial support for this project from the University of Massachusetts Retired Faculty Association and from Consorzio Interuniversitario di Risonanze Magnetiche di Metallo-Proteine (CIRMMP).

Table I Physical and chemical features of M(L-His)$_2$ complexes

Metal	log K_1	log K_2	Geometry	Buffered Metal (ΔG)[f]
Ni(II)	8.43[a]	6.71[a]	Octahedral[b]	-67.5 kJ/mol
	7.81[g]	6.67[g]		
	8.36[h]	7.04[h]		
Co(II)	6.71[a]	5.35[a]	Octahedral[c]	-53.9 kJ/mol
Cu(II)	9.79[a]	7.62[a]	Square-pyramidal[d]	-84.3 kJ/mol
Zn(II)	6.34[a]	5.35[a]	Tetrahedral[e]	-51.8 kJ/mol

[a,] [11]
[b,] [17]
[c,] [23]
[d,] [85]
[e,] [86]
[f,] Value determined using a DYNAFIT simulation to generate species concentrations when $[M]_{total}$ = 1.66 µM, $[L\text{-}His]_{total}$ = 60 µM, and K_1, K_2 values from [11]. ΔG values were calculated using $\Delta G = -(298\ K * 8.314\ J \bullet K^{-1} \bullet mol^{-1})) * \ln([Metal]_{free})$ as in [42].
[g.] [10]
[h] [12]

Table II. Comparison of Ni-coordination features derived from XAS for NiSOD, NiSodN and NiSodN•LHis[70].

Features	**NiSodN**	**Reduced Ni(II)SOD**	**NiSodN•LHis**
1s→3d	Yes	Yes	Yes
1s→4pz	No	Yes	Yes
Coordination	6	4	4-/5
Geometry	Octahedral	Planar	Planar/Pyramidal
Photosensitivity & edge shift	No	No	Yes (0.3 eV)
S → Ni CT	No	Yes	Yes
EXAFS	6 N/O with 1 Imidazole	2 N/O+2 S with 1 Imidazole	2-3 N/O+1/2 S with 1 Imidazole
Spin	High	Low	Low

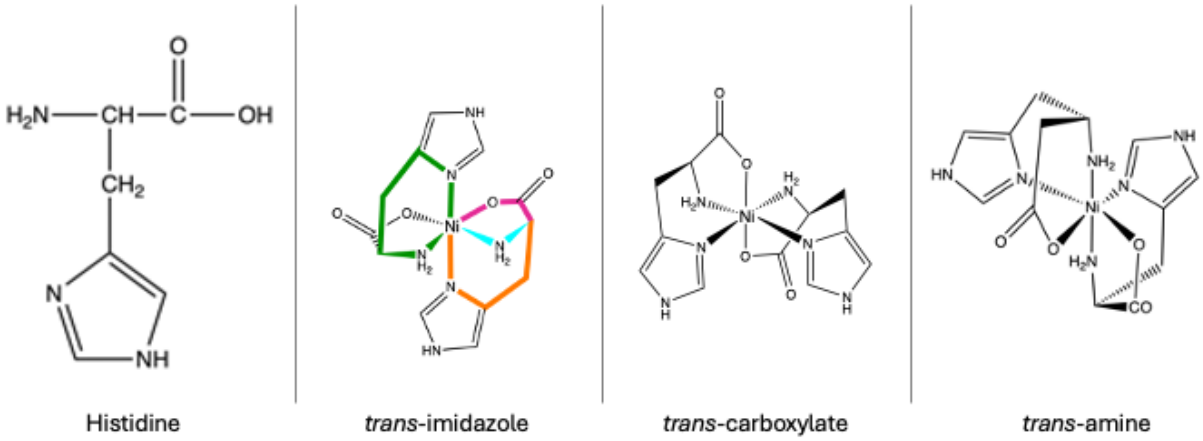

Figure 1. The structures of histidine and the geometric isomers of Ni(L-His)$_2$. (The five-, six-, and seven-membered chelate rings are highlighted in blue+magenta, green, and orange + magenta, respectively.)

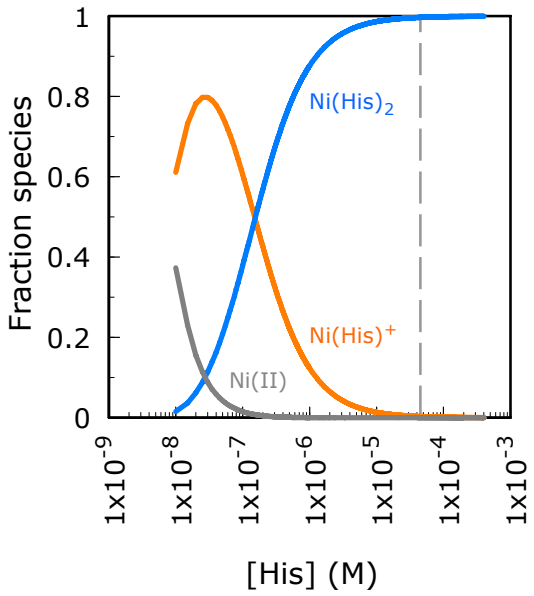

Figure 2. Distribution of Ni(His)n species as a function of $[His]_{total}$. The absolute values of each component at constant $[Ni]_{total}$ = 10 nM was determined using DYNAFIT [87] and published stability constants (see Table 1 and ref [10]). Fraction species distributions were determined algebraically. The vertical dashed line (45 μM His) approximates a lower limit of physiological [His] from several different environments (bacterial cytosol[15,43], human plasma (https://www.sickkids.ca/siteassets/care--services/for-health-care-providers/lab-information-sheets/plasma-amino-acids-reference-ranges.pdf), and human digestive tract)[13].

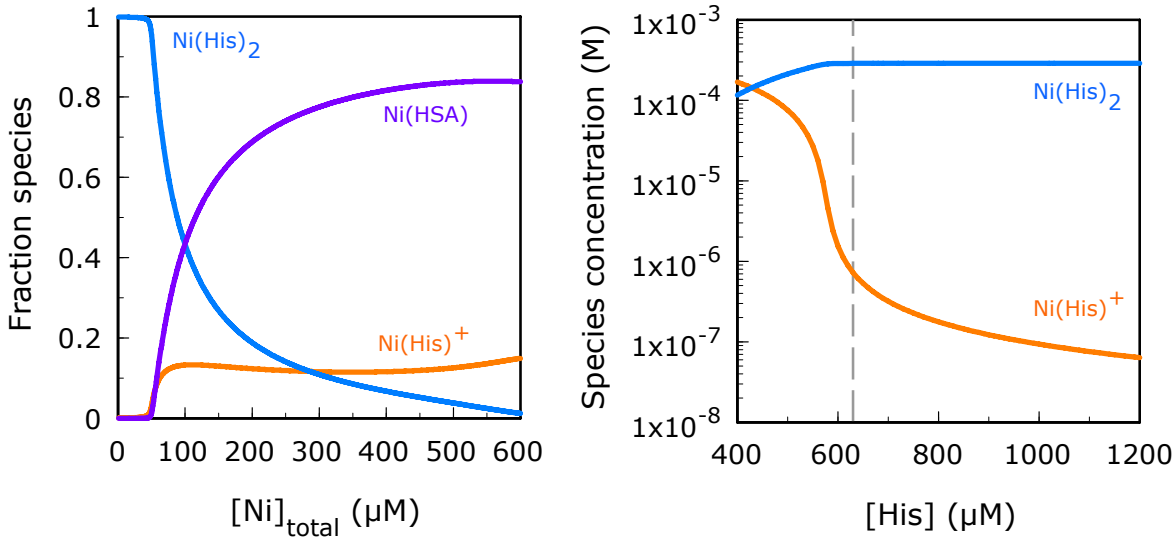

Figure 3. Ni complex speciation based on experimental data for Ni loading of human serum albumin[27]. Simulations were performed using DYNAFIT [87] and published $Ni(His)_n$ stability constants (see Table 1 and ref [10]) and Ni(HSA) stability constant log(*K*) = 5.50 and $[HSA]_{total}$ = 1.73 mM . Left panel, species fractionation highlighting the stability of $Ni(His)_2$ compared to Ni(HSA), where $[His]_{total}$ = 100 μM. Right panel, absolute concentrations of the $Ni(His)_n$ species based on experimental conditions (Figure 3a in ref [27]; variable [His] and $[Ni(II)]_{total}$ = 288 μM). Vertical dashed line (630 μM His) was the estimated lower [His] limit used in the Ni-loading experiments

\

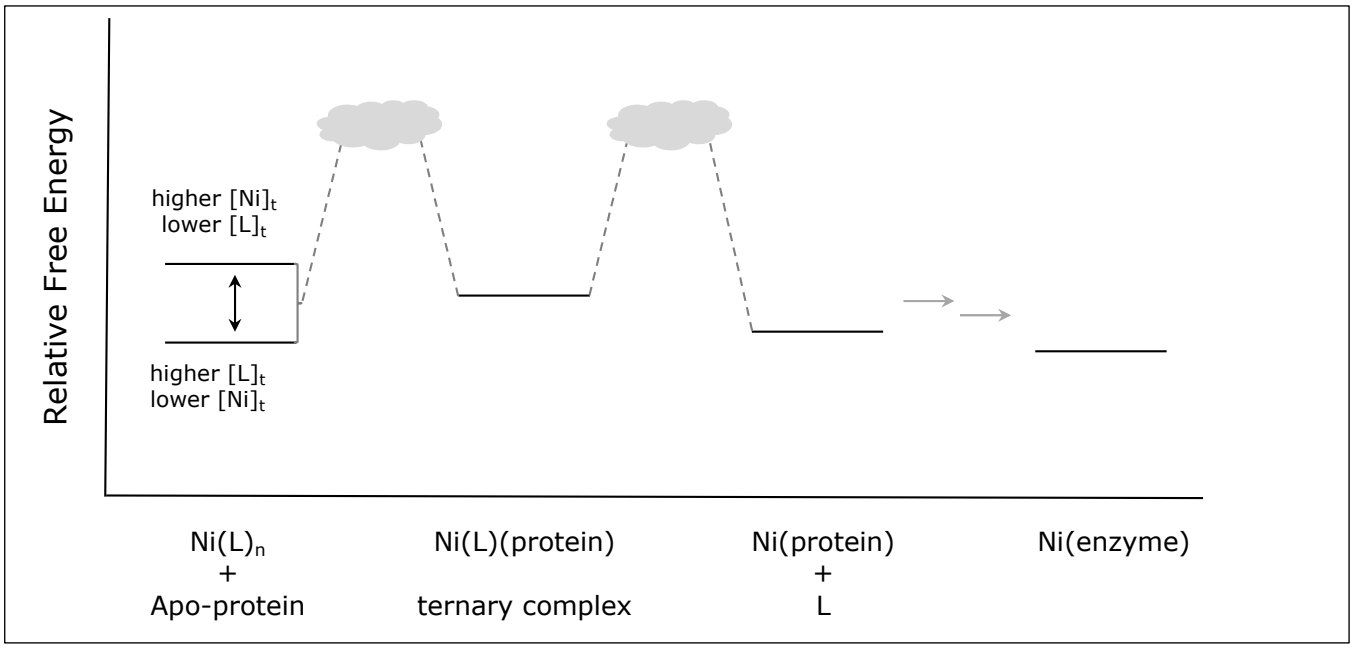

Figure 4. Illustrative reaction coordinate scheme for Ni-transfer between a LMW complex and a protein binding site. The ΔG and ΔE_a values are for visualization purposes only.

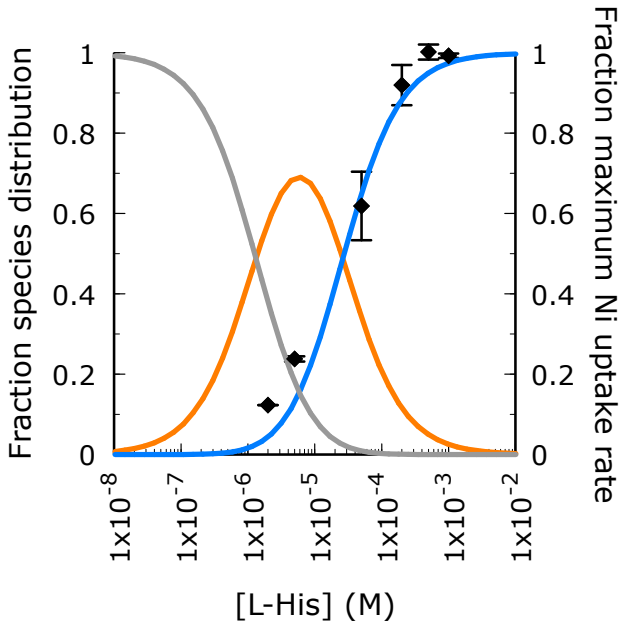

Figure 5. NikABCDE-dependent Ni(II)-uptake in *E. coli* depends on $Ni(His)_2$ abundance. Figured adapted from ref. [16], which describes the collection of the experimental data for ^{63}Ni uptake rate (black diamonds) and simulation of speciation of Ni_{free} (grey line), $Ni(His)^+$ (orange line), and $Ni(His)_2$ (blue line).

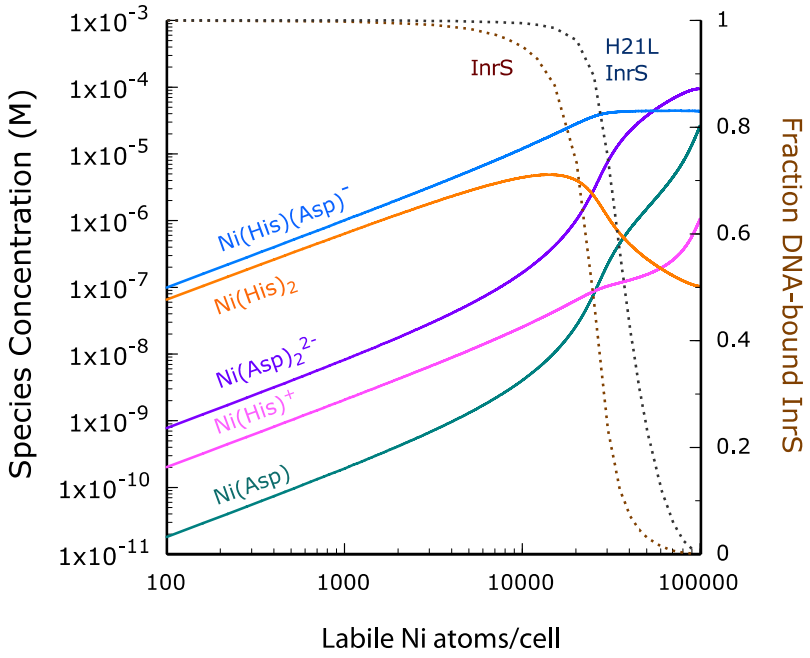

Figure 6. Modeling the transcriptional response of *Synechocystis* InrS as a function of LMW Ni complex speciation. The following parameter values were used from ref [43]: [His], 45 μM, [Asp], 283 μM, and InrS Ni and DNA-affinities (Supplemental Table 2, as dissociation constants (M) for wild-type and H21L, respectively,): K_1, 2.8 x 10^{-12}, 5.5 x 10^{-11} M, K_3, 9.4 x 10^{-9}, 2.1 x 10^{-8} K_4, 2.3 x 10^{-6}, 2.7 x 10^{-6}). Parameter values and quantitative models used are as described in the text. DYNAFIT was used to determine LMW Ni species concentrations. $Ni(His)_n$ stability constants were from Table 1 (ref [10]) and $Ni(Asp)_n$ (K_1 = 6.81 and K_2 = 5.18) and Ni(His)(Asp) ($K_{2,Asp}$ = 6.24 and $K_{2,His}$ = 7.79) complex stability constants were calculated from Table 2 in ref. [12]. The supplemental spreadsheet from ref [42] was used to model fraction InrS bound at selected buffered [Ni] concentrations from the DYNAFIT simulation. With these parameters, $Ni(H_2O)_6^{2+}$ reaches ≥ 1.6 x 10^{-9} M (threshold of 1/cell) at ~ 50000 total labile Ni atoms/cell.

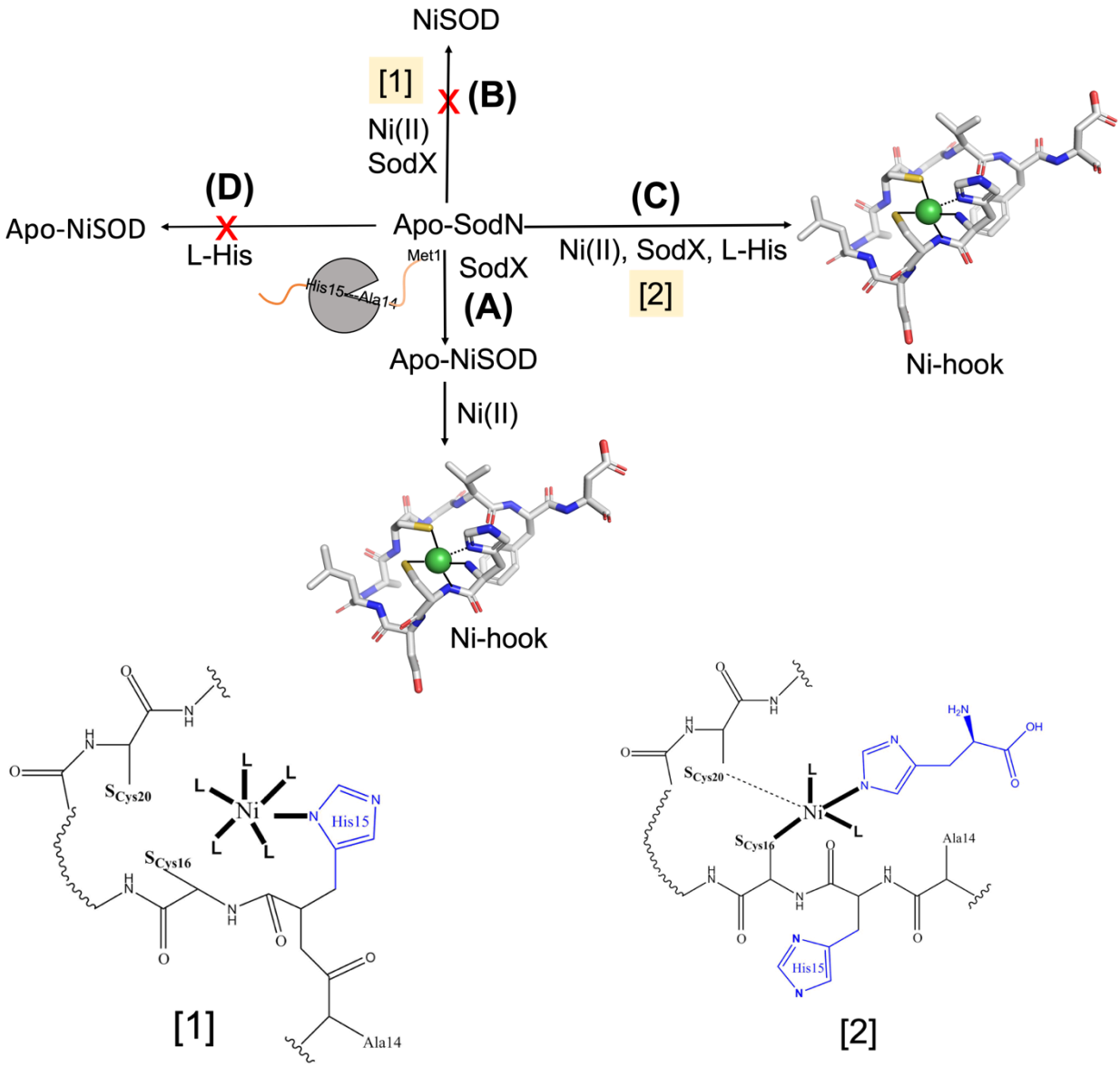

Figure 7. A summary of the proteolytic reaction outcomes affecting NiSOD maturation under different conditions. Yellow encircled highlight depicts a hypothetical structure for the Ni(L-His)SodN complex.

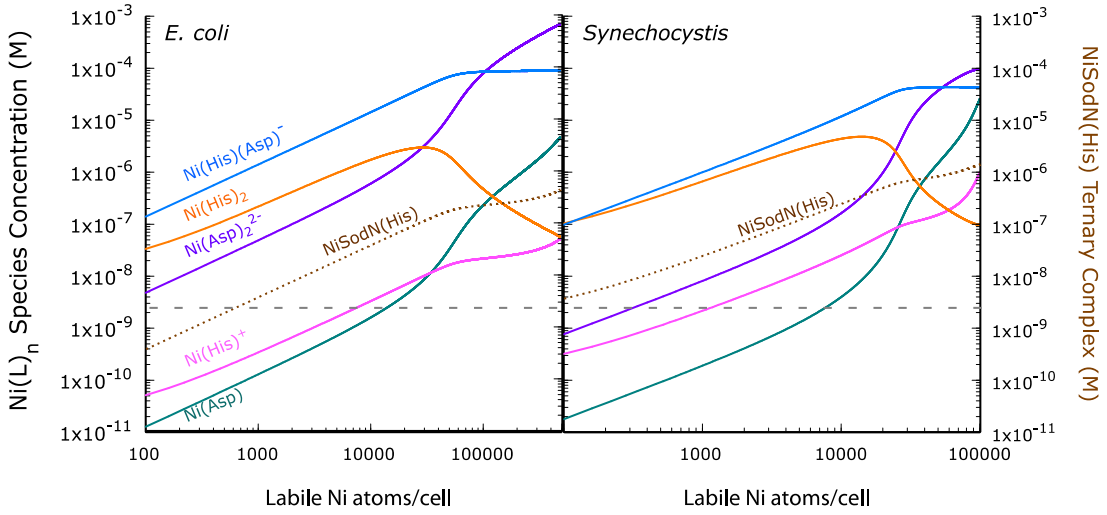

Figure 8. Modelling $Ni(L)_n$ complex speciation and NiSOD(His) ternary complex formation in two different bacterial cytosols. Simulations were carried out using DYNAFIT [87] and published stability constants as in Figure 6. *E. coli* cytosolic $[His]_{total}$ and $[Asp]_{total}$ were set at 90 μM and 2.5 mM, respectively [15].The stability constant for NiSOD(His) was chosen to be the same as K_2 for $Ni(His)_2$ formation (Table 1), with 1000 copies (1.6 μM) of SodN. Horizontal dashed line represents the threshold concentration for one complex/cell (1.66 nM) using *E. coli* cell volume (1 fL) for both plots, as this is a reasonable approximation for *Synechocystis*.

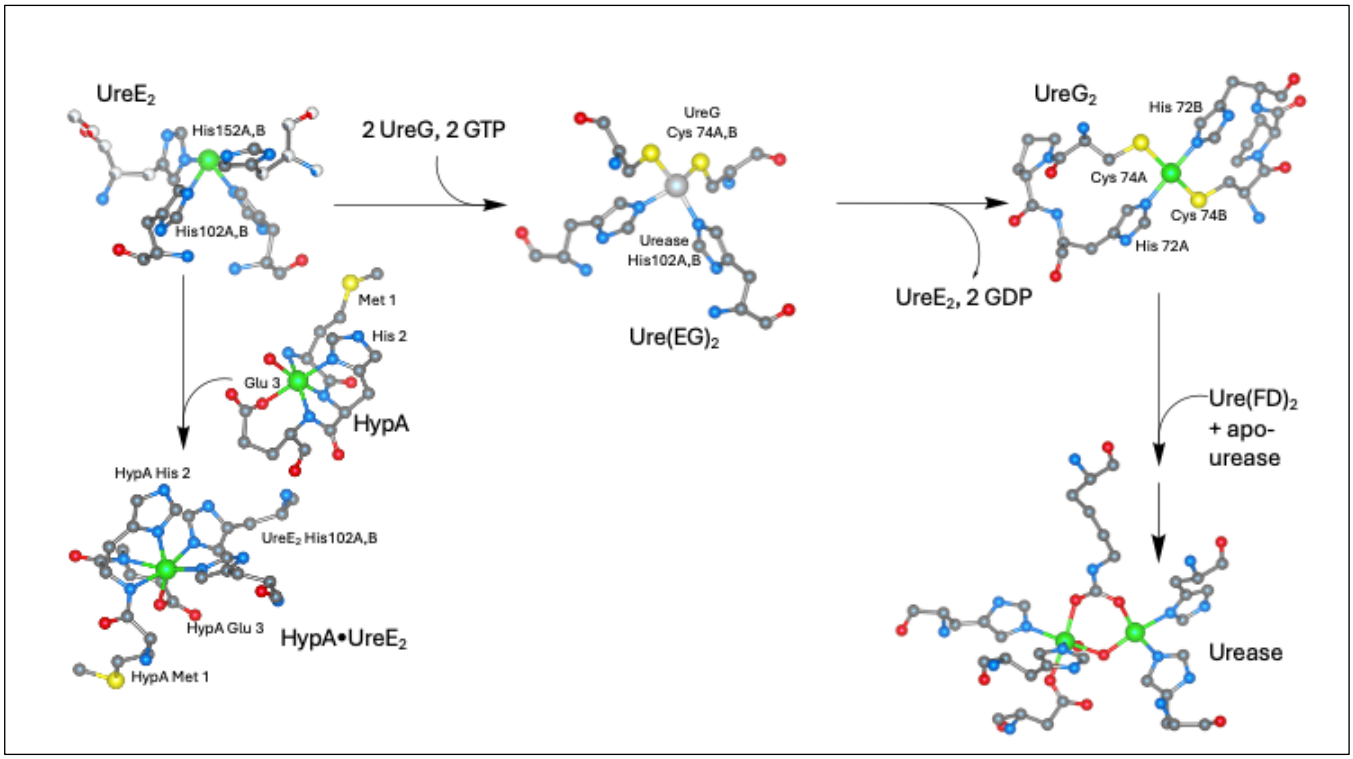

Figure 9. The role of histidine coordination in urease maturation. $UreE_2$ (upper left) forms a complex at the dimer interface that involves coordination of two pairs of histidine residues. Dimeric $UreE_2$ forms complexes with HypA (lower left) and with dimeric $UreG_2$ (center) that maintain coordination of the pair of histidine residues on the surface of $UreE_2$. Hydrolysis of GTP drives an allosteric change that completes the transfer of Ni(II) from $UreE_2$ to $UreG_2$. $UreG_2$ transfers Ni(II) via the $Ure(FD)_2$ complex to apo-urease, where each Ni(II) center is coordinated by a pair of histidine residues. ($UreE_2$ is drawn from a combination of crystallographic (PDBID 3TJ8)[59] and x-ray spectroscopic data as described in the text[59]. The Hyp A structure is derived from a combination of NMR studies (PDBID 6G81)[70], x-ray spectroscopy and mutagenesis[70]. The HypA•$UreE_2$ complex is a computational model supported by NMR and x-ray spectroscopic data[68]. The $Ure(EG)_2$ structure is a computational model with the metal binding site modeled as a Zn(II) complex[55,64]. The $UreG_2$ structure is drawn from crystallographic data (PDBID 5XKT)[61], as is the structure of

the urease active site (PDBID 1EJX). The figure was constructed using VESTA for visualization[88]).